Journal of Catalysis 270 (2010) 172–184

Contents lists available at ScienceDirect

Journal of Catalysis

journal homepage: www.elsevier.com/locate/jcat

Selectivity in sorption and hydrogenation of methyl oleate and elaidate on MFI zeolites

An Philippaerts [a], Sabine Paulussen [a,1], Stuart Turner [b], Oleg I. Lebedev [b], Gustaaf Van Tendeloo [b], Hilde Poelman [c,2], Metin Bulut [a], Filip De Clippel [a], Pieter Smeets [a], Bert Sels [a,*], Pierre Jacobs [a,*]

[a] COK KU Leuven, 23 Kasteelpark Arenberg, B-3001 Heverlee, Belgium
[b] EMAT University of Antwerp, 171 Groenenborgerlaan, B-2020 Antwerpen, Belgium
[c] Department of Solid State Sciences, Surface Physics and Thin Films, Ghent University, 281 Krijgslaan, S1, B-9000 Gent, Belgium

ARTICLE INFO

Article history:
Received 8 September 2009
Revised 2 December 2009
Accepted 25 December 2009
Available online 27 January 2010

Keywords:
Methyl oleate
Methyl elaidate
Removal *trans* fatty acid methyl esters
Pt/ZSM-5 zeolites
Selective sorption
Selective hydrogenation
Oleochemistry
Vegetable oil conversion
Pt clusters

ABSTRACT

Different zeolites were tested for selective removal of methyl elaidate (*trans* isomer) from an equimolar mixture with methyl oleate (*cis* isomer). Sorption experiments of the geometric isomers show that only ZSM-5 samples with reduced Al content in the framework are able to discriminate among the bent *cis* and the linear *trans* fatty acid methyl esters. Hydrogenation experiments of equimolar methyl oleate and elaidate mixtures at low temperature (65 °C) and high hydrogen pressure (6.0 MPa), using Pt catalysts, confirm this result. Only with a Pt/Na–ZSM-5 catalyst outspoken selectivity for the hydrogenation of the *trans* isomer is obtained. In order to prepare a selective Pt/ZSM-5 catalyst, the influence of Pt addition (impregnation, ion-exchange and competitive ion-exchange) and Pt activation (different calcination and reduction temperatures) on the Pt-distribution and Pt particle size was investigated using SEM, bright-field and HR TEM, EDX, electron tomography, CO-chemisorption, XPS, XRD, and UV–vis measurements. The best result in terms of hydrogenation activity and selectivity is obtained with a Pt/ZSM-5 catalyst, which is prepared via competitive ion-exchange, followed by slow calcination up to 350 °C under high O_2 flow and a reduction up to 500 °C under H_2. This preparation method leads to a Pt/ZSM-5 catalyst with the best Pt distribution and the smallest Pt clusters occluded in the zeolite structure. Finally, the influence of zeolite crystal size, morphology, and elemental composition of ZSM-5 on hydrogenation activity and selectivity was investigated in detail.

1. Introduction

Vegetable oils, like soybean oil, consist of triglyceride molecules, composed of three fatty acids attached to a glycerol backbone [1]. Whereas in naturally occurring molecules, the fatty acids have an even number of C atoms, they can occur with different chain lengths and different numbers of double bonds. The most common fatty acid chains in vegetable oils consist of 18 carbon atoms, containing between 0 and 3 double bonds, *viz.* stearic (C18:0), oleic (*c*C18:1), linoleic (*c*C18:2), and linolenic acid (*c*C18:3), the geometric configuration of natural fatty acid residues in triglycerides being *cis* w.r.t. the double bonds.

Catalytic hydrogenation of vegetable oils is a well-known process in food industry to make the oil more resistant against air autoxidation. For physiological reasons, it is desirable to hydrogenate *c*C18:3 chains, unstable against autoxidation, into *c*C18:2 and *c*C18:1, with limited formation of C18:0. Commercial hydrogenation is often conducted with a Ni catalyst between 180 and 200 °C using hydrogen pressures in the range of 50–250 kPa [2], resulting not only in saturation of double bonds, but also in formation of significant amounts of positional and geometric isomers. The presence of *trans* isomers in the fatty acid chains of edible oils, *viz.* elaidate (*t*C18:1), are legally restricted for dietary reasons [3–5]. Main efforts from industry to obtain products low in *trans* include: (1) changes of the hydrogenation parameters [2,6], (2) use of noble metal catalysts containing Pt and Pd [7,8], (3) use of catalytic transfer [9,10], electrocatalytic hydrogenation [11–13] and hydrogenation in supercritical conditions [14–17], (4) use of alternative processes and feeds, including chemical [18,19] and enzymatic interesterification [20], fractionation [21], and (5) use of naturally stable oils low in linolenic acid [22,23].

One aim of the present research is to investigate the fundamental basis for selective removal of *trans* isomers from a hydrogenated/stabilized oil sample via sorptive and size exclusion

* Corresponding authors. Fax: +32 16 321998.
E-mail addresses: bert.sels@biw.kuleuven.be (B. Sels), pierre.jacobs@biw.kuleuven.be (P. Jacobs).
[1] Present address: VITO, Boeretang 200, B-2400 Mol, Belgium.
[2] Present address: Department of Chemical Engineering and Technical Chemistry, Ghent University, 281 Krijgslaan, S5, B-9000 Gent, Belgium.

0021-9517/$ - see front matter © 2010 Elsevier Inc. All rights reserved.
doi:10.1016/j.jcat.2009.12.022

phenomena. This investigation was done at the level of the methyl esters of the fatty acids which in practice are obtained via a simple base catalyzed transesterification of triglycerides with methanol. Zeolites are obvious candidates for such studies. Possibly, the zeolite pore structure will allow to discriminate among the linear *trans* and the bent *cis* chain of the fatty acid methyl ester, *viz.* methyl elaidate (ME, C18:1 *trans*-9) and methyl oleate (MO, C18:1 *cis*-9), respectively.

Second, selectivity in the co-hydrogenation of MO and ME was examined on platinum loaded on zeolites. Pt was chosen as the active metal because of its low double bond isomerization characteristics [24,25]. Ideally, only *trans*-methyl esters of fatty acids should enter the pores of the zeolite and be hydrogenated selectively on the intracrystalline metal phase. The *cis* isomers, with a larger diameter, would be excluded from the pores and thus from the hydrogenation function.

Work is in progress investigating the possibility of extrapolating the concepts from fatty acid methyl esters to triglycerides.

2. Experimental

2.1. Materials

The origin and properties of zeolite supports used, *viz.* commercial and home-made zeolites, are shown in Table 1. Zeolites with different topology, pore size and pore architecture, crystal size, and Si/Al-ratio was selected. γ-Alumina was from Aldrich (type 507C) with a specific surface area of 200 m^2/g. Chemicals used for zeolite synthesis were from Acros. $Pt(NH_3)_4Cl_2$ was from Strem Chem. Methyl oleate and methyl elaidate were from Sigma–Aldrich with a purity of more than 99%.

2.2. Synthesis of ZSM-5

Synthesis of ZSM-5 zeolites according to a published procedure [26] was done with colloidal SiO_2 (LUDOX® AS-40, 40 wt.% suspension in water) as Si-source, $Al(NO_3)_3{\cdot}9H_2O$ as Al-source, tetrapropylammonium (TPA) bromide as templating agent and 1-hexanol/water mixtures as solvent. To a first solution with the following molar composition:

$$(SiO_2)_{1.00}(TPA)_{0.07}(hexanol)_{2.99}(H_2O)_{16.00}$$

a second solution containing various amounts of $Al(NO_3)_3{\cdot}9H_2O$ and NaOH in water was added under stirring so as to obtain a solution with the following molar composition:

$$(Na_2O)_x(AlO_2)_y(SiO_2)_{1.00}(TPA)_{0.07}(hexanol)_{2.99}(H_2O)_{32.00}$$

The values for x and y can be extracted from Table 2.

The solution was then placed in a Teflon autoclave and heated in a Milestone Microsynth Microwave oven for 17 h at 170 °C. Table 2 gives an overview of the compositions of the synthesis solutions for the different ZSM-5 samples. After synthesis the crystals were washed three times with distilled water and calcined in a muffle furnace for 24 h at 550 °C in order to remove occluded organics. XRD analysis confirmed that all samples were 100% crystalline w.r.t. a standard ZSM-5 sample. A combination of yield determination of the synthesis with chemical analysis of the obtained powder indicated that the synthesis efficiency both on Si and Al basis was always around 100 ± 5%. Sample notation involves the zeolite name, preceded by the name of the charge compensating cation and followed by the Si/Al framework ratio, *viz.* Na–ZSM-5(138). A capital C in the sample notation stands for a commercial sample, while MW refers to a lab synthesis in a microwave oven, as described previously.

2.3. Synthesis of Pt catalysts

Pt was introduced in the different supports via three different techniques, *viz.* incipient wetness impregnation (IWI), ion-exchange (IE) or competitive ion-exchange (CIE).

For IWI, an amount of a 0.0427 M aqueous solution of $Pt(NH_3)_4Cl_2$ with volume equal to the total water sorption capacity of a *vacuo*-dried zeolite (0.5 mL/g) was added dropwise to the dry zeolite powder. The catalyst powder was then dried overnight at 110 °C.

IE was done under stirring for 48 h of a zeolite in water slurry, containing the required amount of Pt-precursor in a 200-mL aqueous solution (usually 0.128 mM) per gram of dry zeolite. Prior to metal loading, calcined zeolites were brought in the Na-form via two successive room temperature ion-exchange steps lasting for 16 h. Two hundred milliliters of an aqueous 1 M NaCl solution per gram of dry zeolite was used. After each exchange, the filtration residue is washed three times with distilled water and dried at 100 °C. To achieve a complete Na ion exchange, prior to ion-exchange calcined as-synthesized samples were dropped into aqueous ammonia solutions of pH 10, followed by thorough washing with bidistilled water till neutral pH in the washing waters.

During CIE, the Pt ion-exchange was done in presence of Na ions (NaCl), using a Na/Pt atomic ratio of 25.

The metal content of the exchange solution after reaction was determined by Inductively Coupled Plasma Atomic Absorbance

Table 1
Origin and characteristics of used zeolite supports.

Entry	Zeolite type	Topology	Pore size[a]/dimensionality	Si/Al	Crystal size (μm)	Origin
1	Y	FAU	12MR/3D	2.7	2–3	Zeolyst
2	USY	FAU	12MR/3D	40.0	0.3–0.5	Zeolyst
3	Beta	BEA	12MR/3D	9.9	0.2–0.4	Zeocat
4	Mordenite	MOR	12MR/1D	6.2	1–2	Zeocat
5	Mordenite	MOR	12MR/1D	11.0	1–2	Zeocat
6	Mordenite	MOR	12MR/1D	100.0	1–2	Zeocat
7	L	LTL	12MR/1D	3.9	1	Zeocat
8[c]	ZSM-5	MFI	10MR/2D	40.0	0.3–1.0	Zeolyst
9	ZSM-5	MFI	10MR/2D	78.0	0.5–2.0	Zeolyst
10[d]	ZSM-5	MFI	10MR/2D	138.0	0.4–4.0	Zeolyst
11[b]	MCM-22	MWW	10MR/3D	15.0	2.0–3.0	[48]
12[b]	ZSM-22	TON	10MR/1D	51.0	2.0–3.0	[49]
13[b]	ZK-5	KFI	8MR/3D	2.3	0.4–0.8	[50]

[a] *x*-Membered ring (number of O- or T-atoms atoms circumscribing the main channels).
[b] Home-made according to published procedures.
[c] Sample Na–ZSM-5(C40) in Table 9.
[d] Sample Na–ZSM-5(C138) in Table 9.

Table 2
Composition of solutions used for ZSM-5 synthesis in microwave (MW).

Sample	Si/Al	Na/Al
MW-40	40	24.0
MW-80	80	8.0
MW-100A	100	10.0
MW-100B	100	33.0
MW-150	150	15.0
MW-250A	250	2.5
MW-250B	250	82.6
MW-500	500	4.8

(ICP-AA). In case of normal ion-exchange, no Pt could be detected, while very low Pt levels (<0.10 mg/L) were measured after CIE.

Pt-loaded catalysts are activated by a successive calcination and reduction at 350 and 500 °C, respectively. Prior to activation, the dry powders were compressed, crushed, and sieved, the 0.25–0.50 mm fraction being retained for further use. Calcination was conducted under flowing oxygen (120 mL/g/min), whereas reduction was done under flowing hydrogen (120 mL/g/min) applying heating rates of 0.3 °C/min and 0.4 °C/min, respectively. After calcination, the catalysts were cooled to room temperature under flowing nitrogen. After reduction, the acid sites formed by the reduction of Pt^{2+} to Pt^0 were neutralized in a flow of 5% dry ammonia in N_2.

In the notation of the Pt ion-exchanged samples, the amount and nature of the occluded metal was preceding the zeolite sample notation, while the Si/Al-ratio is given in brackets. A sample denoted as 0.5Pt/Na–ZSM-5(138) was loaded with 0.5 wt.% of Pt and has a Si/Al ratio of 138.

2.4. Catalyst characterization

SEM images of gold-coated samples were taken with a Philips XL series XL 30 FEG, the energy of the incident electron beam being 30 keV.

For transmission electron microscopy (TEM) investigation, the catalyst samples were prepared by suspending the powder materials in methanol and subsequently placing a few drops of the suspension on holey carbon-coated Cu-grids.

Bright-field TEM, high-resolution TEM, and electron diffraction experiments were performed on a Philips CM20 operated at 200 kV. Particle size distributions of the Pt particles were measured from the obtained electron micrographs assuming a spherical morphology of the particles, averaging over 50 particles. EDX analysis was performed using an Oxford EDX detector and Inca analysis software.

Electron tomography experiments were performed on a JEOL 3000F TEM-STEM microscope operated at 300 kV and equipped with a −70° to +70° tomography tilt stage and holder. Images for tomographic reconstruction were taken using a 2° interval, over the largest possible angle, *viz.* 132°. A reference image at 0° tilt was taken before and after image acquisition, to ensure changes in the sample structure were absent due to beam damage during acquisition. Tomographic reconstruction was performed using the TOM Tomography Toolbox [27]. High-angle annular dark field scanning transmission electron microscope (STEM) images were taken using a Technai G2 microscope operated at 200 kV at a nominal spot size of 0.2 nm. The HAADF inner collection semi-angle was 90 mrad. For all techniques, low-intensity beam conditions (lowest possible magnification, low beam intensity and long exposure times) were used as much as possible to minimize the electron dose and possible beam damage of the supported metal particles [28]. The images for the tomographic acquisition were taken in bright-field TEM instead of the HAADF-STEM mode. Although unwanted diffraction contrast inevitably occurs with this technique, use of bright-field TEM was required for the tomography images as prolonged STEM illumination can damage soft porous materials [28].

X-ray photoelectron spectroscopy (XPS) measurements were performed with a Perkin–Elmer PHI ESCA 5500 system, using monochromatic 450 W Al Kα radiation. Despite the low Pt concentration, both the Pt*4f* and the weaker Pt*4d* signals were clearly visible. As the more intense Pt*4f* photolines coincide with the Al*2p* peak, the weaker but isolated Pt*4d* photolines around 315 eV were used to calculate atomic Pt/Si ratios. The oxidation state of Pt is normally extracted from the position of the strongest photoline, *viz.* Pt*4f*. The binding energies of the $Pt4f_{7/2}$ for various oxidation states are well documented, *viz.* 71, 74 and 74.5–75 eV for Pt^0, Pt^{2+}, and Pt^{4+}, respectively [29]. Because of the overlap of $Pt4f_{7/2}$ with Al*2p*, the distinct $Pt4d_{5/2}$ photoline was used to calculate the position of the overlapped $Pt4f_{7/2}$ line. Reference measurements on Pt foil were used to determine the exact distance between the two Pt lines ($\Delta E_b = 243.6 \pm 0.1$ eV).

X-ray diffraction (XRD) measurements were performed on a STOE Stadi P instrument in transmission mode using Cu Kα radiation. On one hand, these measurements were done in order to confirm the zeolite structure and crystallinity after zeolite synthesis and catalyst preparation. On the other hand, the diffractograms were used to check for possible sintering of Pt, which can be evaluated from the Pt diffraction peaks at $2\theta = 39.6$ (111), $2\theta = 45.9$ (200) and $2\theta = 67.3$ (220).

Platinum dispersions were determined using CO-chemisorption. Catalyst pellets loaded in a tubular reactor were reduced according to the pretreatment procedures described previously and cooled down to room temperature under flowing He. For the titration of the Pt surface, pulses of 5 μL of pure CO were added to a He flow of 10 mL/min at an interval of 2 min. The CO concentration in the outlet stream was followed continuously via ion monitoring at $m/e = 28$ with a Pfeiffer Omnistar quadrupole mass spectrometer. For the calculation of the dispersion, adsorption of 1 CO per accessible Pt atom was assumed. The size of Pt particles, d_{Pt}, was derived from the Pt dispersion, D_{Pt}, assuming a cubic particle shape [30]:

$$d_{Pt} = 0.821\left(\frac{1}{D_{Pt}}\right)$$

In situ UV–vis–NIR spectra in the diffuse reflectance mode (DRS) of the series of Pt/ZSM-5 samples oxidized at increasing temperature were recorded on a Varian Cary 5 UV–vis–NIR spectrophotometer. Sample pellets of 0.25–0.5 mm were brought into quartz flow cells, equipped with a suprasil window for DRS measurements. After calcination at different temperatures in a pure oxygen flow of 120 mL/g/min at a heating rate of 0.3 °C/min, the samples were cooled under He and scanned at RT. The spectrum of reference white $BaSO_4$ was subtracted from all Pt/ZSM-5 spectra.

Room temperature chromatographic adsorption experiments in the HPLC mode were conducted with hexane as the mobile phase using a column (4.6 × 45.0 mm) packed with zeolite pellets in the Na-form but devoid of Pt, previously dried at 450 °C. Twenty microliters of the adsorbate (MO or ME) was injected in the mobile phase and passed over the zeolite column. Concentration changes at the column outlet were monitored with a refractive index (RI) detector. The response curve was analyzed by the method of moments [31], the first moment or mean retention time of the pulse being identical to the adsorption equilibrium constant, *K*, which reflects the affinity of the sorbate compound for the adsorbent concerned. A high value for *K* implies that the adsorbate shows a significantly higher affinity for the adsorbent than for the mobile phase. The ratio of the adsorption equilibrium constants of ME and MO (K_{ME}/K_{MO}) corresponds to the selectivity ratio or separa-

tion factor, α. Sorbents characterized by a separation factor higher than one are assumed to adsorb preferably methyl esters of *trans*-monounsaturated fatty acids over the corresponding *cis* isomers.

2.5. Hydrogenation reactions

Hydrogenation of equimolecular mixtures of MO and ME was carried out in 10-mL batch autoclaves. The autoclave was loaded with 5 g of a mixture containing 2 wt.% of substrate in octane and the prereduced dry catalyst. The reaction mixture was homogenized under stirring at 500 rpm with a magnetic stirring bar. After flushing the reaction mixture with N_2, the temperature was raised to 65 °C and 6.0 MPa of H_2 was added. Unless stated otherwise, after 15 min of reaction the autoclave was flushed again with N_2.

After screening of the different catalysts in a 10-mL autoclave, some were tested in a 100-mL Parr-autoclave in the same conditions of temperature and pressure. The reaction mixture was stirred mechanically at 500 rpm. Samples withdrawn from the reactor at certain time intervals, allowed following the reaction progress over time.

2.6. Product analysis

The fatty acid methyl esters (FAMEs) were analyzed with a Hewlett Packard HP 6890 gas chromatograph using a split injection system with split ratio of 100:1 and N_2 as carrier gas. A 60-m highly polar column of the type BPX-70 (SGE) with an internal diameter of 320 μm and a film thickness of 0.25 μm was used for separation. The initial column temperature was kept for 40 min at 180 °C, and then raised at 10 °C/min to 260 °C and held there for 5 min. The FID detector used was kept at 280 °C. For quantification, heptadecane was added as standard.

The hydrogenation degree was also followed by determining the iodine value (IV) of the products. IV values, *viz.* g of iodine consumed per 100 g of fat substrate, were obtained from GC analysis. The ΔIV, the difference between the initial IV, *viz.* 85.7 for a 50/50 mixture of ME/MO, and the end IV, is a measure of the number of double bonds saturated during the reaction and hence a measure of the degree of hydrogenation.

Representation of the catalytic data was done in terms of conversion of ME (X_{ME}) or MO (X_{MO}) or in terms of ΔIV, or in terms of initial hydrogenation activity (after 15 min) per Pt atom. First-order rate constants (k_{ME}, k_{MO}) were obtained from first-order plots of $\ln(X_i)$ over time.

3. Results and discussion

3.1. Zeolite effects on sorption selectivity of methyl oleate and elaidate

In Table 3, an overview of room temperature adsorption equilibrium constants (K_{ME}, K_{MO}) and selectivity ratios (α) of ME over MO is shown for different adsorbents. γ-Alumina shows low values for K_{MO} and K_{ME}. This should be attributed to the weak interactions between the adsorbate and the support. An α-value of 0.99 points to the absence of selectivity in the adsorption of any of the two geometric isomers.

Different Na–ZSM-5 samples with MFI topology (entries 6–8) show α-values exceeding a value of 1.00. They increase with increasing Si/Al-ratio up to an α value of 6.6 for a Si/Al-ratio of 138, thus pointing to increasingly preferred adsorption of ME over MO. The higher values for both K_{MO} and K_{ME} in ZSM-5 zeolites with higher Si/Al-ratios and comparable crystal sizes, can be rationalized by the increasing hydrophobicity of the samples. The higher the Si/Al-ratio, the more hydrophobic is the zeolite and thus the more likely it is that the apolar fatty acid chains will enter the pores. Next to this polarity effect, an increase in Si/Al-ratio is also accompanied by a decrease in pore diameter as the Al–O bond length is larger than the Si–O bond length [32]. This decrease in pore diameter can also result in enhanced sorption selectivity. The ZSM-5 structure seems to be most promising. Even the more aluminous ZSM-5 show superior sorption constants for both isomers compared to other 10MR zeolites, *viz.* with MWW and TON topology (entries 9 and 10), pointing to a restricted access. It seems that participation in the sorption of the half-cages at the external surface of MCM-22 is not significant.

Table 3
Overview of adsorption equilibrium constants, K_i, and selectivity ratio, α, of methyl elaidate (ME) and methyl oleate (MO) in Na-exchanged zeolites.

Entry	Zeolite	Topology	Si/Al	K_{ME}	K_{MO}	α
1	Y	FAU	2.7	8.77	9.73	0.90
2	USY	FAU	40.0	5.25	5.36	0.98
3	Beta	BEA	9.9	25.90	29.20	0.89
4	Mordenite	MOR	6.2	0.98	1.03	0.95
5	L	LTL	3.9	0.68	0.74	0.92
6	ZSM-5	MFI	40.0	3.23	3.08	1.05
7	ZSM-5	MFI	78.0	6.09	5.08	1.20
8	ZSM-5	MFI	138.0	25.37	3.85	6.59
9	MCM-22	MWW	15.0	1.25	1.24	1.01
10	ZSM-22	TON	51.0	2.34	2.21	1.06
11	ZK-5	KFI	2.3	0.91	0.88	1.03
12	γ-Alumina	/	/	1.01	1.00	0.99

Whereas the 12MR zeolites (entries 1–5) all have α-values slightly lower than 1, they show significant variations in absolute values of the adsorption equilibrium constants. This is explained by the larger pore volumes and the better accessibilities of the pores in the 12MR zeolites compared to the zeolites with smaller pore size. Zeolite L and mordenite show low values for K_{MO} and K_{ME} possibly because of high hydrophilicity (low Si/Al-ratios) and reduced dimensionality (monodimensional 12MR). The α values in the 12MR zeolites point to the absence of sorption selectivity.

The 8MR zeolite shows very low adsorption equilibrium constants indeed (entry 11). Narrow pores do not allow access, while the low Si/Al-ratio, probably is at the basis of weak interaction of apolar fatty esters with the external surface of hydrophilic crystals.

Concluding, only ZSM-5 samples with reduced Al content in the framework at room temperature allow to discriminate among methyl elaidate and oleate. From the data, it follows that a combination of pore size, pore dimensionality and Si/Al-ratio is at the basis of this beneficial effect in sorption. Therefore, in the hydrogenation experiments with Pt/zeolites, most emphasis was on ZSM-5 samples, while only the faujasite and mordenite structure has been used for comparative purposes.

3.2. Effect of zeolite structure on hydrogenation activity and selectivity

Pt-loaded catalysts prepared from a limited number of commercial zeolites with different topologies and Si/Al-ratio were tested in a hydrogenation reaction with equimolecular amounts of ME and MO. Pt with its low double bond isomerization activity [24,25] was chosen as the active metal phase in the hydrogenation catalysts. The characteristics of the commercial supports are given in Table 1, while the results of the hydrogenation reactions with some of them are shown in Table 4.

Pt ion reduction in zeolites (Z^-) occurs via the following overall equation [33]:

$$\left[Pt(NH_3)_4^{2+}\right]_{1/2}Z^- + \frac{1}{2}H_2 \rightarrow \frac{1}{2}Pt + 2NH_3 + H^+Z^-$$

Z^- representing the negatively charged zeolite framework. The removal of NH_3 ligands and Pt ion reduction occurs via subsequent air calcination and hydrogen reduction. The latter treatments can

Table 4
Performance of 0.5 wt.% of Pt prepared via ion-exchange and subsequent calcinations and reduction on different commercial supports in the hydrogenation of ME in an equimolecular mixture of ME and MO (2.0 wt.% in octane) at 65 °C with 6.0 MPa of hydrogen.

Support	Si/Al	Pt/lipid	ΔIV	Rel. In. Act.[a]	k_{ME}/k_{MO}[b]
Al_2O_3[c]	/	0.025	5.6	20.4	0.91
Na–Y	2.6	0.1	42.5	38.6	0.85
Na–USY	40	0.05	16.3	29.6	0.56
Na–Mor	11	0.2	1.4	0.6	0.70
Na–Mor	100	0.1	14.4	14.0	0.82
Na–ZSM-5	40	0.1	1.1	1.0	1.27
Na–ZSM-5	138	0.1	22.2	20.2	1.27

[a] Initial activity (relative ΔIV per unit amount of Pt in the reactor, calculated after 15 min of reaction) relative to Pt/Na–ZSM-5(40).
[b] Ratio of first-order rate constants of ME over MO hydrogenation over a longer period.
[c] Prepared via impregnation.

be done in different ways using different temperature programs. To minimize acid-catalyzed reactions such as double bond shift and geometric isomerization, it is advisable to neutralize afterward the acid sites formed, *viz.* by treatment with gaseous dry ammonia (see Section 2).

The hydrogenation activity on the 0.5Pt/zeolite catalysts prepared via ion-exchange varies significantly (Table 4). Zeolites Y and mordenite are known to accept all Pt in the intracrystalline space of a 0.5Pt/zeolite sample prepared via ion-exchange [34]. Although not of prime importance in this work, the high hydrogenation activity with 0.5Pt/NaY is the result of good accessibility of the intracrystalline Pt particles. This is less the case in the 0.5Pt/Mor(11) sample with reduced pore size and pore dimensionality. The reduced activity of 0.5Pt/Na–USY w.r.t. 0.5Pt/Na–Y is in line with its decreased sorption capacity due to mesopore formation during ultrastabilization of zeolite Y. The increased activity of dealuminated mordenite is probably the result of enhanced accessibility of the structure upon dealumination. The low activity of ZSM-5 should be related to the low pore size and reduced accessibility. The difference in activity of the two ZSM-5 samples cannot be rationalized at this stage, but is probably related to difference in Pt location/dispersion and will be treated in more detail.

As in this work the goal is to manipulate hydrogenation selectivity, the catalysts with a selectivity ratio $k_{ME}/k_{MO} > 1$ are of primary importance. They belong to the ZSM-5 family of catalysts.

When the Pt particles are assumed to be very accessible, the selectivity should be in favor of the *cis* isomer, *viz.* MO. It is clear that the *cis*-olefin double bond of MO, in a non-constrained environment will form more easily a π-complex with the metal surface compared to the *trans*-form of ME. Therefore, further attempts to improve the hydrogenation selectivity in favor of ME, will focus on Pt/ZSM-5 materials as catalyst.

3.3. Effect of Pt addition to Na–ZSM-5(C-138) on hydrogenation activity and selectivity

The chromatographic adsorption experiments show that the pore structure of siliceous ZSM-5 is able to discriminate among the methyl elaidate straight chain and the methyl oleate bent chain, at least in chromatographic conditions. Therefore, selective hydrogenation of ME in presence of MO could be feasible, provided the Pt metal clusters are accommodated fully in the intracrystalline voids of the Na–ZSM-5 zeolite. Pt clusters located on the outer surface of the zeolite crystals, will not allow this shape selective hydrogenation reaction to occur.

The different preparation methods described in the experimental section, *viz.* incipient wetness impregnation (IWI), ion-exchange (IE), or competitive ion-exchange (CIE), were tested to prepare the most selective Pt/Na–ZSM-5(C-138) catalyst for the hydrogenation of an equimolecular mixture of MO and ME. In order to minimize the number of Pt clusters located on the outer surface of the zeolite, competitive ion exchange with $Pt(NH_3)_4Cl_2$ may be suitable [35,36]. If IE occurs in absence of a competitive ion, the Pt metal ion preferably will be located in the outer rim of the crystals, given the strong electrostatic interaction between the ligated Pt^{2+} ions and the negative charges of the lattice and the excess of sites present w.r.t. the number of Pt ions involved. The addition of an excess of competitive cation, *viz.* Na^+, forces the Pt ions to be positioned across the whole crystal, thus leading after reduction to a more homogeneous distribution of metal particles throughout the zeolite. However, data illustrating this effect only exist for zeolite Y and mordenite [35,36].

In order to determine the nature of the superior catalyst preparation method, 0.5 wt.% of Pt was incorporated in the Na–ZSM-5(C-138) zeolite by means of IWI, IE-350, or CIE, followed by calcination under oxygen at 350 °C and subsequent hydrogen reduction at 500 °C (Table 5). Fast heating could lead to incomplete oxidation of ammonia and hence autoreduction of the Pt-precursor. Also, at higher heating rates, there will be more water left in the zeolite, which will coordinate to the Pt-cations, enhancing their mobility in the zeolite and leading to a lower dispersion [37].

The crystallinity of the catalysts as examined by X-ray diffraction at various stages during the preparation, *viz.* after Pt addition and pretreatment, remained unchanged (data not shown). No reflection peaks of Pt^0 were observed for the three samples (IWI, IE, and CIE).

The most important characteristics of the three 0.5Pt/Na–ZSM-5(C-138) samples are summarized in Table 5, entries 1–3. The table shows that the Pt dispersion as calculated from CO measurements is higher in the ion-exchanged samples (IE-350 and CIE, entries 2 and 3) compared to the impregnated sample (IWI, entry 1). The size of the Pt clusters increases in the sequence IE < IE-350 < IWI. These observations are not in line with results from a previous re-

Table 5
Preparation methods and characterization of Pt in a 0.5Pt/Na–ZSM-5(C-138) catalyst.

Entry	Catalyst	Calcination (°C/h)	Reduction (°C/h)	D_{Pt}[a] (%)	d_{Pt}[b] (nm)	d_{Pt}[c] (nm)	E_b[d] (eV)	Pt/Si[d] ($\times 10^{-3}$)
1	IWI	350/1	500/1	23	3.6	7.6 ± 4.5		
2	IE-350	350/1	500/1	38	2.2	2.0 ± 0.8	71.2	2.89
3	CIE	350/1	500/1	40	2.0	1.7 ± 0.8	70.8	3.06
4	IE-NC	−/−	500/1					
5	IE-200	200/9	500/1					
6	IE-250-1	250/6	500/1			2.4 ± 0.9	71.3	2.99
7	IE-250-2	250/6	250/8			1.7 ± 0.6	70.8	8.80

[a] Pt dispersion from CO measurements.
[b] From CO measurements.
[c] From TEM.
[d] From XPS measurements using the Pt$4d_{5/2}$ and Si$2p$ eV lines for Pt and Si, respectively.

port in which smaller Pt clusters were obtained by impregnation compared to ion-exchange of a K–ZSM-5 zeolite [38]. According to the authors, this observation is related to the presence of additional potassium species in the pores of the impregnated zeolite, which would hinder the migration of platinum to form larger particles. However, in Pt/Na–Y catalysts, ion-exchange has been reported to lead to smaller Pt clusters, located in the pores of the zeolite, while impregnation gave large Pt clusters agglomerated on the outer surface [39]. The ZSM-5 sample loaded via CIE (entry 3, Table 5) shows the highest Pt dispersion and hence the smallest Pt particles. This enhancement is in line with previous reports about competitive ion-exchange in zeolite Y [35] and mordenite [36].

In the corresponding SEM images (Fig. 1), no Pt particles could be detected for catalyst IWI, IE-350, or CIE, indicating that either no Pt clusters or only very small Pt nanoclusters are present on the outer surface of the zeolite crystals.

In order to further characterize the influence of the Pt addition on the Pt-distribution, XPS measurements were performed. As can be seen from Table 5, the Pt/Si ratio is similar for IE-350 and CIE (entries 2 and 3). Assuming that all Pt initially present in the exchange solution becomes associated with the zeolite crystals, corresponding to a bulk Pt/Si atom ratio of 1.52×10^{-3}, the values indicate that there should be Pt enrichment on the surface. The XPS analysis of the various catalysts is also informative on the Pt oxidation state. As the binding energies of Pt$4f_{7/2}$ are around 71 eV, Pt should be in the metallic state, irrespective of the preparation method.

Bright-field TEM experiments were performed on all catalyst samples (Fig. 2). Pt clusters are visible in all samples, the size of the Pt particles and their distribution across the different crystals depending on the loading mechanism used. TEM measurements clearly show that impregnation leads to an asymmetric broad Pt-distribution (IWI, Fig. 2a), peaking at 8 nm and ranging from 2 to 20 nm. As expected for the impregnation method, many particles should be located outside the zeolite crystal in agreement with a previous report [39].

In the ion-exchanged samples (Fig. 2b and c), the Pt clusters are distributed more homogeneously as is obvious from the narrower particle size distribution and show smaller mean Pt-cluster size in agreement with the CO-chemisorptions results. TEM images of IE-350 and CIE generally show rather narrow Pt-distribution with mean Pt-cluster size of 1.7 nm (Table 5). Occasionally, some spots are found representing large Pt clusters. The Pt size distribution plot of IE-350 shows a slightly higher maximum at 2.0 nm. The chemical nature of the metal nanoparticles present is evidenced by EDX for all samples. An illustrative spectrum is shown in Fig. 2d.

Even though the presence of the Pt particles can be evidenced by TEM and EDX analysis, the positioning of the clusters within the crystal matrix cannot unequivocally be established. To show a more detailed image of the smallest Pt clusters, high-resolution (HR)TEM pictures are shown for the two ion-exchanged samples in Fig. 3. The HRTEM images show the presence of small Pt clusters in the zeolite materials. Occasionally, some larger nanoparticles (see e.g. Fig. 5) are positioned at the surface of the zeolite crystals. Assuming that these small, low-contrast particles are not at the external surface of the zeolite crystals, but incorporated into the crystal lattice of the zeolite matrix, it should be realized that they have sizes that exceed the pore intersection diameter of the MFI topology, *viz.* ± 0.55 nm. Similar results have been observed earlier via EXAFS [38,39] and also have been assigned to intracrystalline Pt clusters at locally destroyed lattice spots.

Electron tomography revealed no further information about the localization of the small nano-sized Pt particles (<2 nm) as these reliably could not be observed with this technique due to both the low contrast difference between the zeolite matrix and the smallest particles as well as the resolution limit in bright-field TEM tomography with a limited tilt angle, which lies around 2 nm [40].

Finally, the three 0.5Pt/Na–ZSM-5(C-138) samples prepared via IWI, IE, and CIE were used as catalyst in the competitive hydrogenation of an equimolecular mixture of ME and MO (Table 6, entries 1–3). The results from the hydrogenation reactions at ΔIV values of 5 and 10 vary in a way similar to that of the CO dispersion mea-

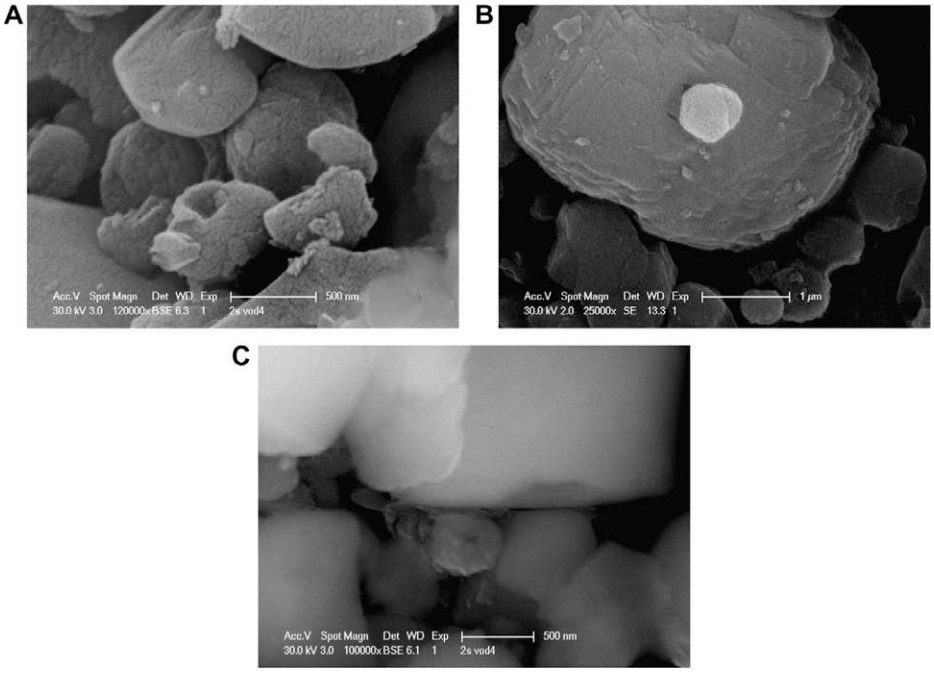

Fig. 1. SEM images of catalysts 0.5Pt/Na–ZSM-5(C-138) prepared via (A) incipient wetness impregnation of Pt, IWI; (B) ion-exchange, IE-350; (C) competitive ion-exchange, CIE.

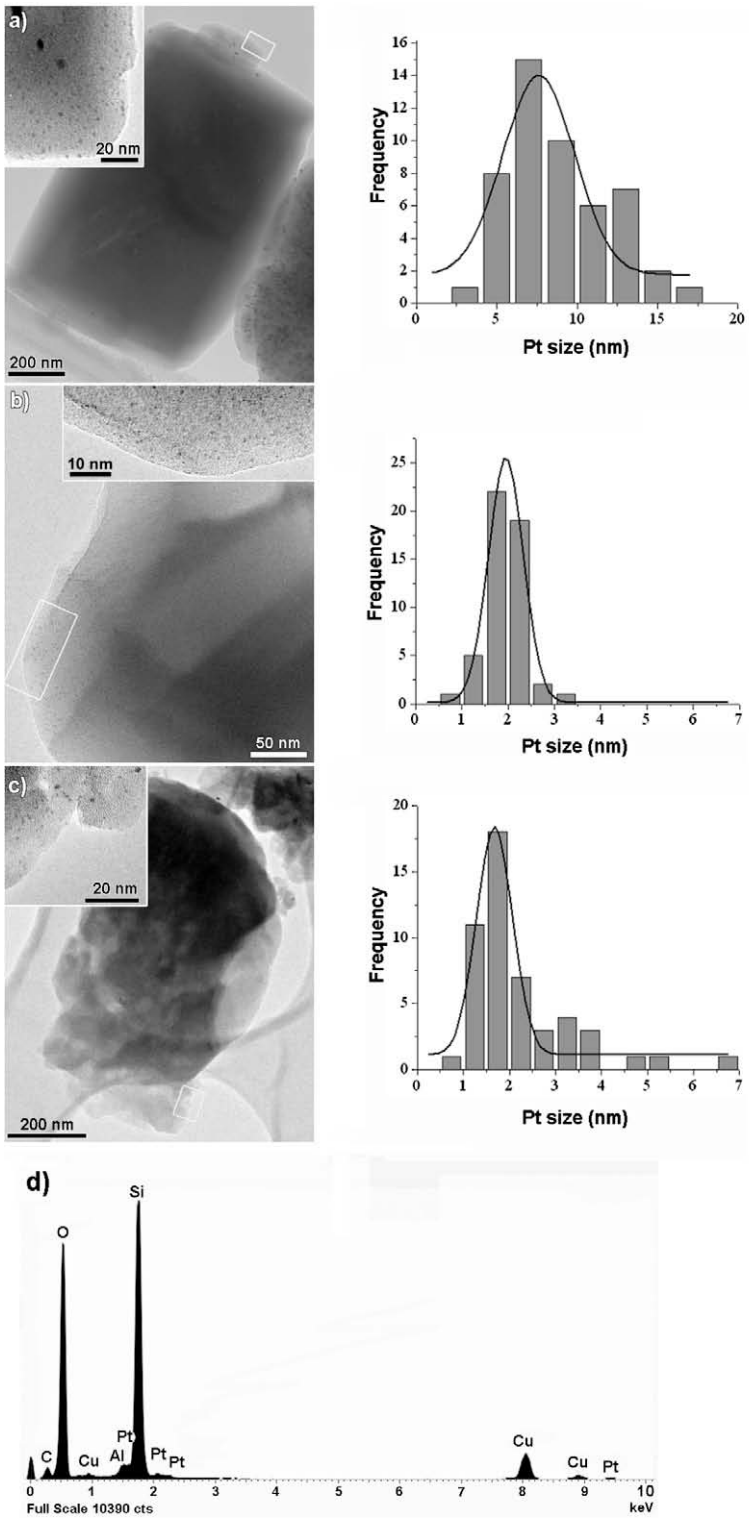

Fig. 2. Bright-field TEM images of 0.5Pt/Na–ZSM-5(C-138) catalysts prepared via different Pt adsorption methods and the corresponding Pt size distributions (measured from obtained transmission electron micrographs assuming a spherical morphology of the particles): (a) IWI (large zeolite crystals almost devoid of Pt particles and small crystals densely loaded with Pt particles (inset)); (b) IE-350; (c) CIE. The insets are magnified versions of the regions indicated by the white rectangles. (d) Typical EDX spectrum of the catalyst (IE-350).

surements. Indeed, the sequence of activities of the ZSM-5 catalysts (CIE > IE-350 > IWI) is the same as for the metal dispersion. Next to the effect on hydrogenation activity, the preparation method has a major impact on the hydrogenation selectivity. At $\Delta IV = 5$, the ion-exchanged samples (IE-350 and CIE) show a preference for the hydrogenation of ME, while samples prepared via IWI hardly shows any selectivity. At $\Delta IV = 10$, the ion-exchanged samples retain their preference for ME hydrogenation, while for the impregnated IWI catalyst the selectivity switches, MO being hydrogenated preferentially. This observation points to the pres-

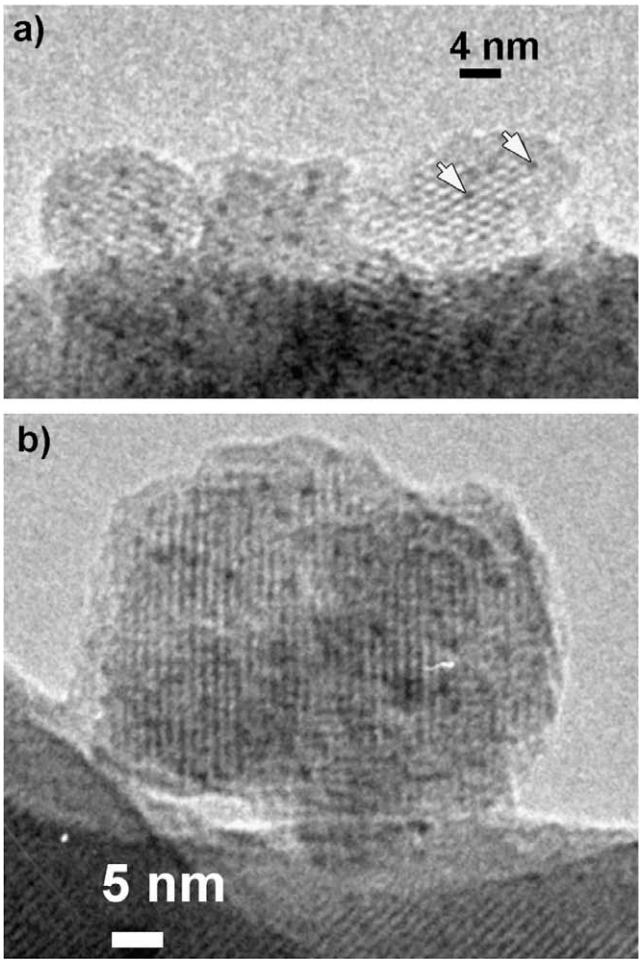

Fig. 3. High-resolution TEM images of 0.5Pt/Na–ZSM-5(C-138) catalysts prepared via (a) IE-350; (b) CIE. Pt particles with good contrast are clearly visible in all images.

ence of intracrystalline Pt for preparations IE-350 and CIE. The lack of selectivity observed for IWI preparation, indicates that a majority of a-selective Pt particles are formed on the outer surface of the zeolite.

Conclusively, the ion-exchanged samples (IE-350 and CIE) have smaller (intracrystalline) Pt clusters compared to the impregnated sample (IWI). The former are more uniformly distributed throughout the zeolite crystals, leading to higher activity and selectivity for the hydrogenation of ME w.r.t. MO. The sample prepared via competitive ion exchange shows the highest dispersion and hydrogenation activity. The ion-exchanged samples show the highest selectivity because of the increased contribution of intracrystalline Pt.

3.4. Effect of Pt/Na–ZSM-5 activation on hydrogenation activity and selectivity

An ion-exchanged sample of 0.5Pt/Na–ZSM-5(C-138) was subjected to different thermal pretreatments as shown in Table 5 (entries 2, 4–7). Comparison of IE-NC (no calcination), IE-200 (calcination at 200 °C), IE-250-1 (calcination at 250 °C), and IE-350 (calcination at 350 °C) indicates that for an identical reduction temperature (500 °C), the precalcination temperature has a pronounced effect on the final activity (Table 6). The lower the calcination temperature, the lower is the activity. In contrast to the calcination temperature, the reduction temperature (after an optimal preoxidation) seems to have no influence on the activity (see IE-250-1 and IE-250-2). In previous work, it was shown that the calcination temperature was determining the PtO dispersion and consequently the Pt dispersion after reduction [38].

The selectivity at ΔIV of 5 and 10 are compared in Table 6. The sample precalcined at 350 °C and reduced at 500 °C (IE-350) has the highest selectivity, while the lowest selectivity is obtained with IE-NC and IE-200. These data are again in agreement with the hypothesis that a high Pt-distribution is a prerequisite for selective hydrogenation of ME in presence of MO.

Previous studies have shown that calcination prior to reduction is important in stabilizing small metal particles in ZSM-5 [41,42].

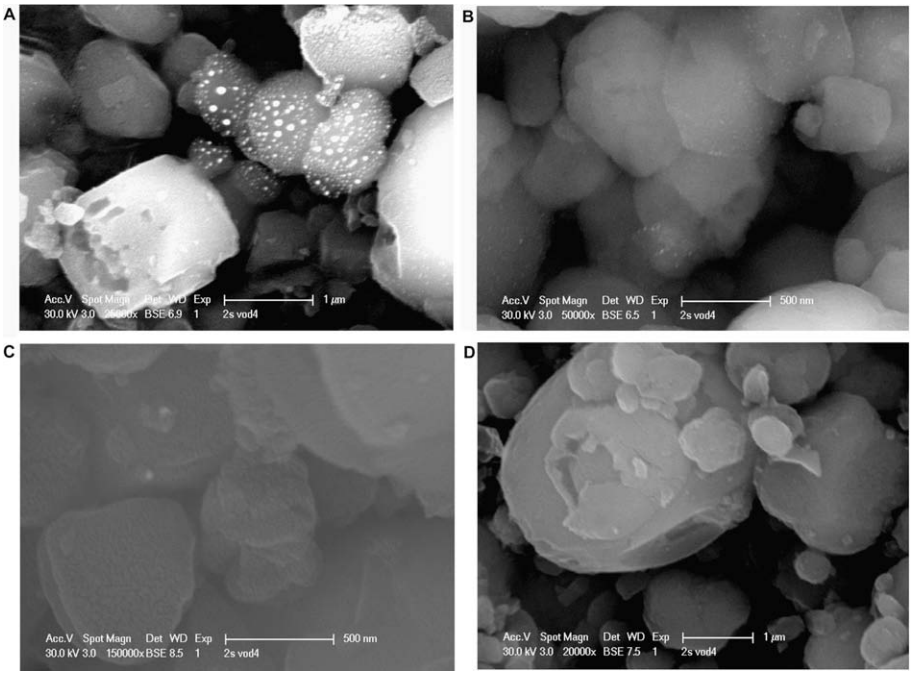

Fig. 4. SEM images of the 0.5Pt/Na–ZSM-5(C-138) catalysts after preoxidation and standard reduction: (A) IE-NC; (B) IE-200; (C) IE-250-1; (D) IE-250-2.

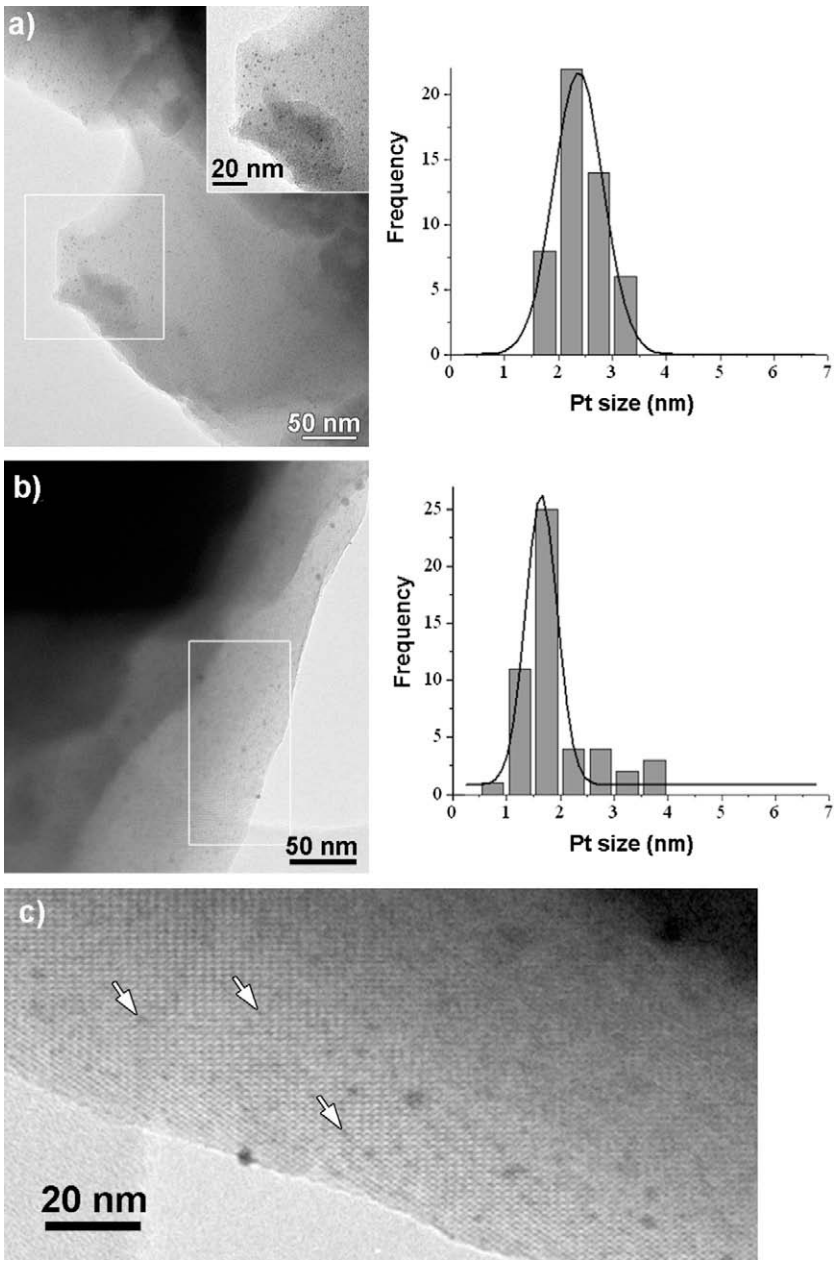

Fig. 5. Bright-field TEM images and the corresponding Pt size distributions (measured from obtained transmission electron micrographs assuming a spherical morphology of the particles) of 0.5Pt/Na–ZSM-5(C-138) catalysts: (a) IE250-1 and (b) IE250-2 with enlarged inset in image (a) corresponding to the region indicated by the white rectangle. (c) HRTEM image corresponding to the region indicated by the white rectangle in image (b).

Table 6
Performance of differently prepared Pt/Na–ZSM-5(C-138) catalysts in the hydrogenation of a 2.0 wt.% equimolecular mixture of methyl oleate and methyl elaidate in octane.[a]

Catalyst[b]	ΔIV = 5 (10)			Initial activity (mol mol Pt^{-1} s^{-1})[c]
	X_{ME} (%)	X_{MO} (%)	X_{ME}/X_{MO}	
IWI	6.0 (10.4)	5.8 (13.1)	1.0 (0.8)	7.90
IE-350	6.4 (12.7)	5.4 (10.8)	1.2 (1.2)	11.54
CIE	6.2 (12.5)	5.5 (11.0)	1.1 (1.1)	20.71
IE-NC	2.4 (–)	8.9 (–)	0.3 (–)	2.34
IE-200	3.9 (–)	7.9 (–)	0.5 (–)	4.91
IE-250-1	–(11.1)	–(11.9)	–(0.9)	8.94
IE-250-2	5.1 (10.2)	6.5 (12.9)	0.8 (0.8)	8.78

[a] 65 °C, 60 bar, Pt/lipid = 0.05 wt.%.
[b] Same as in Table 4.
[c] Calculated after 15 min of reaction.

When the calcination step was omitted and a Pt/ZSM-5 sample was directly reduced in hydrogen, a marked migration of Pt to the outer surface of the zeolite occurred with the growth of large Pt clusters (12–15 nm). The results obtained with IE-NC are in agreement with these observations. From the SEM image in Fig. 4a large Pt clusters (up to 150 nm) exhibiting high contrast with the zeolite crystals are easily detected, leading to reduced activity and selectivity for *trans* reduction (Table 6). The SEM images of IE-200 (calcined at 200 °C) also show a large fraction of outer surface Pt clusters (Fig. 4b) albeit somewhat smaller in size, while no Pt clusters could be detected with SEM in case of IE-250-1 (Fig. 4c), IE-350 (Fig. 1b) and IE-250-2 (Fig. 4d). The latter samples were further analyzed by TEM, showing good Pt-distributions and small Pt clusters (Figs. 2b and 5) with a mean size around 2.0 nm. The distribution on IE-250-2 (reduced at 250 °C) is more asymmetrical, while also 3–4 nm clusters were observed. The Pt particles are clearly

visible, some being positioned at the surface of the zeolite crystals. The majority of the particles is assumed to be encapsulated in the zeolite crystals.

It seems that not only the calcination temperature, but also the calcination time, the rate of temperature increase and the pretreatment mode, *viz.* with air flow or in static conditions, with pure oxygen or dry air, has an influence on the metal dispersion. In order to obtain small, homogeneously distributed Pt clusters, it is important that the Pt-precursor is totally decomposed and that Pt^{2+} ions are formed before reduction. It has been claimed [43–45] that a pale green color is associated with the presence of Pt^{2+} coordinated to the zeolite framework, while subsequent reduction of such a sample leads to the formation of small Pt particles in Pt/H–ZSM-5 [46]. Sample IE-350 in contrast to IE-200 and IE-250, acquired indeed a light green color after calcination.

UV–vis measurements obtained during the calcination step (Fig. 6), confirm this visual observation. Only after calcination at 350 °C or higher, additional absorption bands at 15,800 and

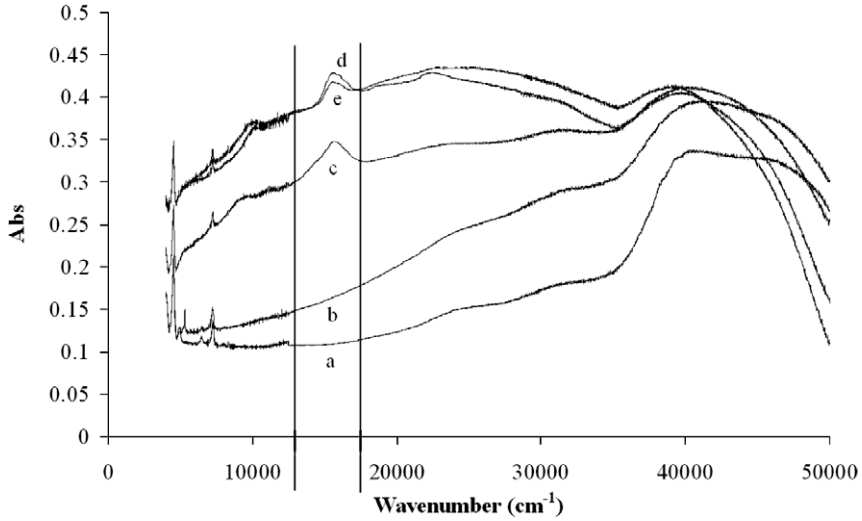

Fig. 6. UV–vis spectra of $[Pt(NH_3)_4]^{2+}$ in 0.5Pt/Na–ZSM-5(C-138), after precalcination at (a) 200, (b) 250 and (c) 350, (d) 400 and (e) 550 °C.

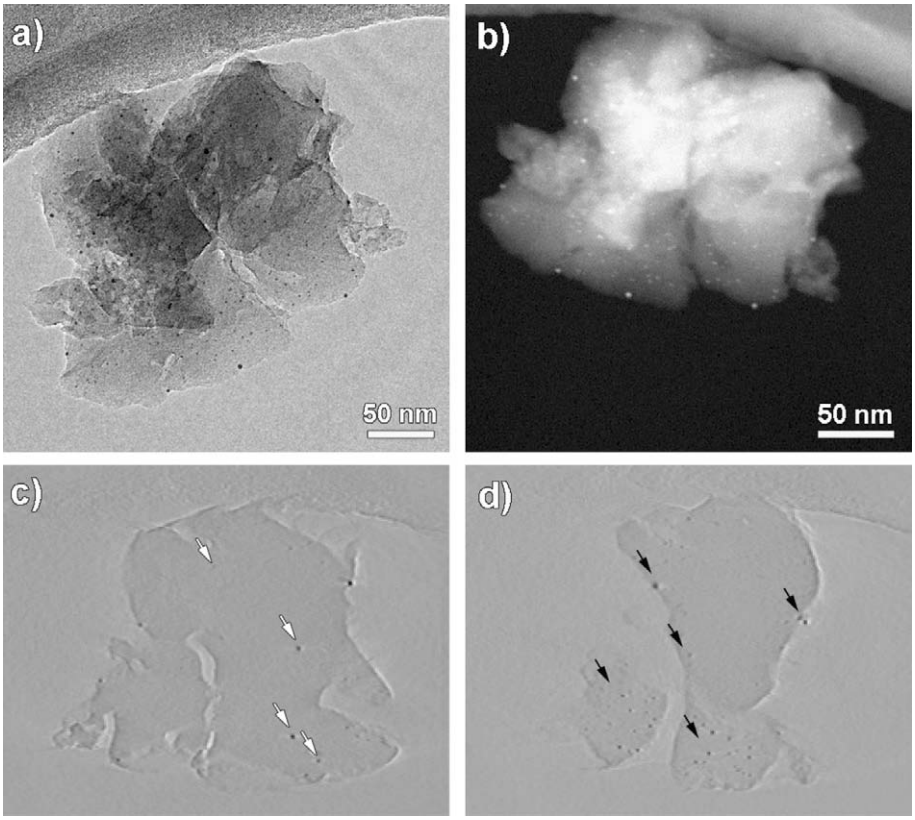

Fig. 7. Electron tomography of catalyst 0.5Pt/Na–ZSM-5(C-138) IE-250-2: (a) bright-field TEM image after oxidation/reduction; (b) HAADF-STEM image; (c and d) slices through the tomographically reconstructed volume of the zeolite matrix; particles are in the bulk of the zeolite or near the surface of the zeolite crystal or on the surface (black arrows). Small particles (<2 nm) from tomographic reconstruction are not visible due to low contrast.

22,000 cm^{-1} were detected. The formation of these bands after O_2 pretreatment previously has been reported for Pt/H–ZSM-5 [46]. The replacement of the NH_3 ligands in the square planar $Pt(NH_3)_4^{2+}$ complex by weaker zeolite lattice O ions also with square planar symmetry, is suggested to result in a shift of the d–d transitions from approximately 35,000 and 43,000 cm^{-1} (hidden under the intense metal-to-ligand charge transfers) to 15,800 and 22,000 cm^{-1}, respectively. This shift points to the complete removal of the NH_3 ligands during O_2 calcination at temperatures higher than 350 °C [46]. As a consequence, severe metal atom agglomeration during the subsequent H_2 reduction via the unstable $Pt(NH_3)_2H_2$ intermediate is prevented [45] and a highly active and selective Pt/ZSM-5 catalyst is obtained.

In contrast to the calcination temperature, the reduction temperature seems to have less influence on the initial activity (Table 6, IE-250-1 and IE-250-2). However, lowering the reduction temperature from 500 to 250 °C has a negative impact on selectivity. XPS measurements (Table 5) indicate that more Pt particles are present on the outer rim of crystals of IE-250-2 (reduction at 250 °C) as evidenced by a higher Pt/Si ratio, compared to IE-250-1 (reduction at 500 °C).

In order to determine the exact position of the Pt clusters within the zeolite crystals, electron tomography was carried out on a selected sample IE-250-2 (Fig. 7) [40,47]. The tomographically reconstructed slices through the zeolite matrix show indeed that most Pt particles are positioned near the surface of the zeolite crystals (Fig. 7c) or are present on their surface. In the smaller zeolite crystals, the particles are distributed more homogeneously (Fig. 7d, bottom). Migration of Pt to the outer surface may be ascribed to the low temperature treatment. As the temperature during calcination and reduction was not higher than 250 °C for IE-250-2, the Pt-precursor is probably not completely decomposed and hence migration to the outer surface of the zeolite crystal is possible. XPS measurements further confirm that in all catalysts Pt is in the reduced form (Pt^0), as they all show the same E_b value around 71 eV (Table 5). So, it seems that a reduction temperature of 250 °C is sufficient to fully reduce Pt^{2+} to the metallic state.

As a conclusion, preparation of selective Pt–ZSM-5 hydrogenation catalysts with good activity results from a subtle interplay of preparation parameters. The best catalyst is obtained by competitive ion-exchange of Na–ZSM-5 with Pt^{2+}, followed by a slow calcination up to 350 °C under high O_2-flow. This procedure ensures that after reduction in H_2, a catalyst with homogeneous Pt-distribution in the zeolite crystals is obtained, which is found to be a key parameter for good selectivity.

3.5. Effect of crystal size, morphology and composition of ZSM-5 on hydrogenation activity and selectivity

Diffusional shape-selectivity of ZSM-5 can be improved using larger crystals, provided the metal phase is accommodated in the intracrystalline volume. The sorption measurements indicated that difference of reactant diffusion is at the origin of the selective hydrogenation. As crystals with a higher ratio of internal to external surface will also have a reduced ratio of external to internal Pt clusters, a further hydrogenation selectivity improvement is expected. On the other hand, larger crystals with longer diffusion pathways for adsorbed molecules are expected to show decreased activity.

Hydrogenation results with 0.5Pt/Na–ZSM-5 with different morphology and crystal size are shown in Table 7. Crystal size changes profoundly affect both activity and selectivity. The coffin-shaped zeolite catalysts prepared from the larger crystals, *viz.* MW-100A and MW-250A, show a reduced activity and an enhanced selectivity compared to the corresponding B samples with comparable Si/Al-ratio. Initially, the A samples show only conversion of methyl elaidate to methyl stearate, while methyl oleate hydrogenation does not occur.

Apart from the crystal size, also the Si/Al-ratio has an influence on the hydrogenation activity, as can be seen in Table 8, where well-formed crystals with different Si/Al-ratios are compared. The effect of the Si/Al-ratio on the initial activity is illustrated in Fig. 8. A maximum for the initial activity is obtained for ZSM-5 catalysts with a Si/Al ratio slightly below 100. The increase of the ME and MO sorption constants with the Si/Al-ratio of the ZSM-5 crystals has been attributed to a decreased polarity or higher hydrophilicity of the zeolite. The same explanation probably holds here. The activity decrease for ZSM-5 with Si/Al-ratios beyond 150, can be related to a decreased amount of intrazeolitic Pt resulting from the decreased number of exchange sites. For example, a zeolite with a Si/Al-ratio of 250 has a maximum CEC corresponding to a 0.64 wt.% Pt^{2+} loading, while for a zeolite with a Si/Al-ratio of 500 it amounts only to 0.32 wt.% Pt^{2+}. Alternatively, part of the

Table 7
Effect of the crystal size and morphology of Na–ZSM-5[a,b] in the selective removal of ME from a 2.0 wt.% equimolar mixture of ME and MO in octane. Hydrogenation reactions were conducted at 65 °C with 6.0 MPa of hydrogen.

Catalyst	MW-100A	MW-100B	MW-250A	MW-250B
Si/Al	100	100	250	250
Crystal size (μm)	3 × 4.5	0.5–1	2.5 × 3.5[c]	2–2.5
Form	Coffin	Spherical	Coffin	Spherical
Pt/lipid	0.4	0.1	0.4	0.4
Time (min)	60	15	15	15
ΔIV	4.7	5.9	0.1	2.8
Rel. In. Act.[d]	0.41	5.37	0.023	0.64
k_{ME}/k_{MO}	3.34	1.23	∞	2.79

[a] 0.5 wt.% Pt on Na–ZSM-5 prepared via CIE with $Pt(NH_3)_4Cl_2$, oxidation at 350 °C and reduction at 500 °C.
[b] Na–ZSM-5 was synthesized according to Table 2.
[c] With less than 10% coffins with a size of 7 × 10 μm.
[d] Relative initial activity (relative ΔIV per unit amount of Pt in the reactor, calculated after 15 min of reaction) w.r.t. the activity of Pt/Na–ZSM-5(C-40) (Table 2).

Table 8
Effect of the Si/Al-ratio in Pt/Na–ZSM-5 on the selective removal of ME in an equimolar mixture of ME and MO. Hydrogenation reactions were conducted at 65 °C, 6.0 MPa of hydrogen using a Pt/lipid molar ratio of 0.4.

Catalyst	MW-40	MW-80	MW-100A	MW-150	MW-250A	MW-500
Size (μm)	5	4.5 × 6.5	3 × 4.5	4 × 10	2.5 × 3.5[a]	2 × 4[b]
Si/Al	40	80	100	150	250	500
Time (min)	15	60	60	60	15	15
ΔIV	0.4	5.7	4.7	4.2	0.1	0.0
Rel. In. Act.[c]	0.091	0.45	0.41	0.25	0.023	0
k_{ME}/k_{MO}	∞	1.79	3.34	3.56	∞	–

[a] Less than 10% crystals with 7 × 10 μm.
[b] Less than 10% crystals with 10 × 15 μm.
[c] Relative initial activity (relative ΔIV per unit amount of Pt in the reactor, calculated after 15 min of reaction) w.r.t. the activity of 0.5Pt/Na–ZSM-5(C-40) (Table 2).

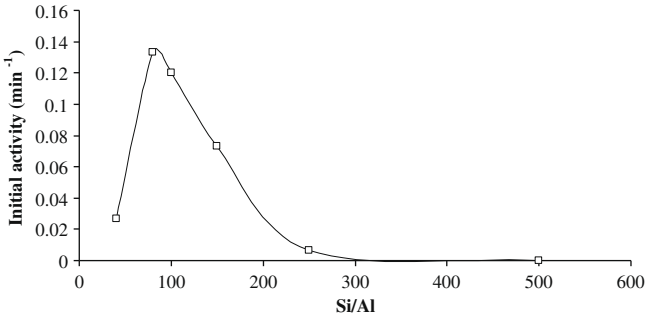

Fig. 8. Effect of the Si/Al-ratio of 0.5Pt/Na–ZSM-5(CIE) on the initial activity during hydrogenation of an equimolecular mixture of methyl oleate and methyl elaidate (conditions of Table 8).

Pt can be hidden deeply in the crystal, where for diffusional reasons MO or ME have no access.

So far only initial activity and selectivity around a ΔIV of 5 has been discussed. In order to investigate the reaction in time, some of the previous catalysts were tested in a 100-mL Parr reactor equipped with on-line sampling device. The results are shown in Table 9. As can be seen, all ZSM-5 catalysts show a preference for the hydrogenation of ME, catalysts MW-80 and MW-150 showing the highest selectivity. In Fig. 9 a comparison is made between the performance of Pt loaded on ZSM-5 samples with different crystal sizes and γ-alumina. The Pt/alumina catalyst shows a small preference for the hydrogenation of MO, while the three Pt/ZSM-5 catalysts show a preferred hydrogenation of ME, the large crystals of MW-80 and MW-150 having the highest preference.

Table 9
Performance of different catalysts in the selective hydrogenation of an equimolecular mixture of ME and MO (2.0 wt.% in octane). Reactions were conducted at 65 °C and 6.0 MPa of hydrogen in a 100-mL Parr reactor with sampling device.

Catalyst	Pt/Al_2O_3	C-40[c]	C-138[d]	MW-80	MW-150
Size (μm)	–	0.3–1	0.4–4	4.5 × 6.5	5.5 × 7
Si/Al	–	40	140	80	150
wt.% Pt	0.5	1	0.5	1	0.5
Pt/lipid	0.015	0.375	0.05	0.2	0.2
Rel. In. Act.[a]	42.44	0.73	17.64	0.32	0.86
X_{ME}/X_{MO}[b]	0.90	1.40	1.13	1.85	1.92

[a] Relative initial activity (relative ΔIV per unit amount of Pt in the reactor after 15 min of reaction) w.r.t. the activity of Pt/Na–ZSM-5(40) (Table 2).
[b] Conversions at ΔIV = 10 (calculated after fitting a straight line through the origin in a *X* versus ΔIV graph).
[c] Sample from entry 8 in Table 1.
[d] Sample from entry 10 in Table 1.

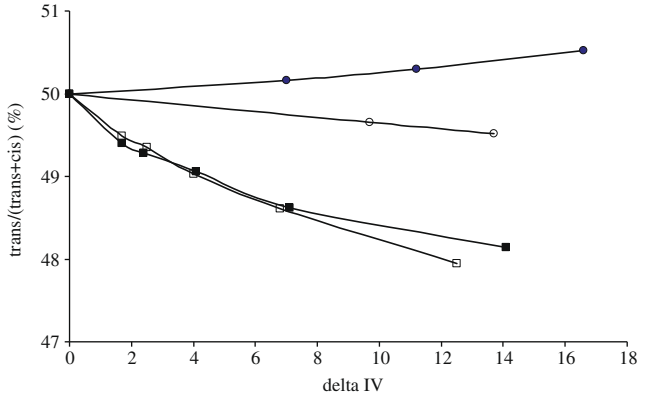

Fig. 9. Selectivity (*trans*/(*trans* + *cis*) over conversion (delta IV) plots 0.5Pt/Na–ZSM-5(C-138) (○) catalysts and 0.5Pt/Na–ZSM-5 prepared via MW-80 (□) and MW-150 (■) and a non-selective Pt/alumina catalyst (●) in the hydrogenation of an equimolecular mixture of ME and MO (2.0 wt.% in octane). Reactions were conducted at 65 °C and 6.0 MPa of hydrogen pressure.

4. Conclusions

The present work shows that the 10MR pores of ZSM-5 are able to distinguish in a room temperature sorption experiment among the linear chain of methyl elaidate and the bent chain of methyl oleate. In other zeolites with 12MR or 8MR, this is not the case.

Furthermore, it is reported that from the zeolite topologies tested, only a Pt/zeolite catalyst with MFI topology can preferably hydrogenate methyl elaidate in a mixture containing its geometric isomer, methyl oleate. This Pt/Na–ZSM-5 catalyst preferably should be prepared via a competitive ion-exchange, followed by a slow calcination up to 350 °C under high O_2-flow and a reduction up to 500 °C. From all the preparation methods tested (variations of Pt addition and Pt activation), it leads to the highest Pt dispersion, hydrogenation activity and selectivity.

High-resolution TEM images clearly indicate the presence of 1–2 nm sized Pt clusters encapsulated in the lattice of the zeolite crystal. However, some larger Pt particles are present, located near or at the crystal surface. It is shown that especially the calcination step is crucial as it allows the Pt-precursors to be completely transformed into Pt^{2+}, with development of a greenish sample color. The critical conditions require application of a low ramping rate (0.3 °C/min), a high oxygen flow (120 mL/min/g) and an elevated calcination temperature (350 °C).

Finally, the use of larger crystals with a Si/Al-ratio up to 80–150 results in further improvement of the (diffusional) shape-selectivity. Na–ZSM-5 samples with lower Si/Al-ratios show lower activities because of their enhanced hydrophilicity. The decreased activity of samples with higher Si/Al-ratios is attributed to the low amount of exchangeable sites available for Pt ion-exchange combined with the slow diffusion of reactants toward the Pt clusters located near the crystals center.

Acknowledgments

A.P. acknowledges the F.W.O.-Vlaanderen (Research Foundation – Flanders) for a doctoral fellowship. The authors acknowledge BELSPO for sponsoring in the frame of a IAP-VI project (federal government), G.O.A. (K.U. Leuven), and the Flemish government for a long term sponsoring (Methusalem, CASAS).

References

[1] P.J. Wan, in: P.J. Wan (Ed.), Introduction to Fats and Oils Technology, AOCS Press, IL, 1991, p. 330.
[2] H.B.W. Patterson, Hydrogenation of Fats and Oils: Theory and Practice, AOCS Press, IL, 1994.
[3] P.M. Clifton, J.B. Keogh, M. Noakes, J. Nutr. 134 (2004) 1848.
[4] D. Mozaffarian, M.B. Katan, A. Ascherio, M.J. Stampfer, W.C. Willett, N. Engl. J. Med. 354 (2006) 1601.
[5] C.D. Hillyer, Inform 18 (2007) 356.
[6] M. Cizmeci, A. Musavi, M. Kayahan, A. Tekin, J. Am. Oil Chem. Soc. 82 (2005) 925.
[7] B. Nohair, C. Especel, G. Lafaye, P. Marecot, L.C. Hoang, J. Barbier, J. Mol. Catal. A 229 (2005) 117.
[8] K. Belkacemi, A. Boulmerka, J. Arul, S. Hamoudi, Top. Catal. 37 (2006) 113.
[9] A. Smidovnik, J. Kobe, S. Leskovsek, T. Koloini, J. Am. Oil Chem. Soc. 71 (1994) 507.
[10] J.W. Ju, W.S. So, J.H. Kim, B.J. Bae, E.N. Choi, Y.H. Kwon, et al., J. Food Sci. 68 (2003) 1915.
[11] G.J. Yusem, P.N. Pintauro, J. Am. Oil Chem. Soc. 69 (1992) 399.
[12] W.D. An, J.K. Hong, P.N. Pintauro, K. Warner, W. Neff, J. Am. Oil Chem. Soc. 75 (1998) 917.
[13] K. Mondal, S.B. Lalvani, Chem. Eng. Sci. 58 (2003) 2643.
[14] J.W. King, R.L. Holliday, G.R. List, J.M. Snyder, J. Am. Oil Chem. Soc. 78 (2001) 107.

[15] E. Ramirez, F. Recasens, M. Fernandez, M.A. Larrayoz, AIChE J. 50 (2004) 1545.
[16] A. Santana, M.A. Larrayoz, E. Ramirez, J. Nistal, F. Recasens, J. Supercrit. Fluids 41 (2007) 391.
[17] C.A. Piqueras, G. Tonetto, S. Bottini, D.E. Damiani, Catal. Today 133 (2008) 836.
[18] G.R. List, E.A. Emken, W.F. Kwolek, T.D. Simpson, H.J. Dutton, J. Am. Oil Chem. Soc. 54 (1977) 408.
[19] G.R. List, T.L. Mounts, F. Orthoefer, W.E. Neff, J. Am. Oil Chem. Soc. 72 (1995) 379.
[20] G.R. List, T. Pellosso, in: G.R. List, D. Kritchevsky, N. Ratnayake (Eds.), Trans Fats in Foods, AOCS Press, IL, 2007, p. 227.
[21] J.E. Hunter, Lipids 41 (2006) 967.
[22] R.D. O'Brien, P.J. Wakelyn, Inform 16 (2005) 677.
[23] G. Talbot, L. Favre, L. Thörig, Inform 18 (2007) 198.
[24] M. Zajcew, J. Am. Oil Chem. Soc. 37 (1960) 473.
[25] G. Cecchi, J. Castano, E. Ucciani, Rev. Fr. Corps Gras 26 (1979) 391.
[26] T. Sano, S. Wakabayashi, Y. Oumi, T. Uozumi, Micropor. Mesopor. Mater. 46 (2001) 67.
[27] S. Nickell, F. Forster, A. Linaroudis, W. Del Net, F. Beek, R. Hegerl, et al., J. Struct. Biol. 149 (2005) 227.
[28] S. Turner, O.I. Lebedev, F. Schroder, D. Esken, R.A. Fischer, G. Van Tendeloo, Chem. Mater. 20 (2008) 5622.
[29] L. Fiermans, R. De Gryse, G. De Doncker, P.A. Jacobs, J.A. Martens, J. Catal. 193 (2000) 108.
[30] M.G. White, Heterogeneous Catalysis, Prentice Hall, Englewood Cliffs, NJ, 1991, p. 88.
[31] Y. Lin, Y.H. Ma, Ind. Eng. Chem. Res. 28 (1989) 622.
[32] J.H.C. Van Hooff, J.W. Roelofsen, in: H. Van Bekkum, E.M. Flaningen, J.C. Jansen (Eds.), Introduction to Zeolite Science and Practice, Elsevier, Amsterdam, 1991, p. 754.
[33] W.J. Reagan, A.W. Chester, G.T. Kerr, J. Catal. 69 (1981) 89.
[34] P. Gallezot, A. Alarcondiaz, J.A. Dalmon, A.J. Renouprez, B. Imelik, J. Catal. 39 (1975) 334.
[35] H.A. Benesi, US Patent 3 527 835, 1970.
[36] F. Ribeiro, C. Marcilly, G. Thomas, C.R. Acad. Sci. Paris 287 (1978) 431.
[37] J. de Graaf, A.J. van Dillen, K.P. de Jong, D.C. Koningsberger, J. Catal. 203 (2001) 307.
[38] F.W.H. Kampers, C.W.R. Engelen, J.H.C. Vanhooff, D.C. Koningsberger, J. Phys. Chem. 94 (1990) 8574.
[39] B. Imre, I. Hannus, Z. Konya, I. Kiricsi, J. Mol. Struct. 651 (2003) 191.
[40] M. Weyland, P.A. Midgley, in: J. Hutchison, A. Kirkland (Eds.), Nanocharacterisation, RSC Publishing, Cambridge, 2007, p. 304.
[41] E.S. Shpiro, G.J. Toleuva, V.A. Zaikovskii, O.P. Tkachenko, T.A. Vasina, O.V. Bragin, K.M. Minachev, in: H.G. Karg, J. Weitkamp (Eds.), Zeolites as Catalysts, Sorbents and Detergent Builders, Elsevier, Amsterdam, 1989, p. 145.
[42] N.I. Jaeger, J. Ratkhousky, G. Sckhulz-Ekloff, A. Svennson, A. Zukal, in: P.A. Jacobs, R.A. van Santen (Eds.), Zeolites, Facts, Figures, Future, Elsevier, Amsterdam, 1989, p. 1005.
[43] E.S. Shpiro, R.W. Joyner, K.M. Minachev, P.D.A. Pudney, J. Catal. 127 (1991) 366.
[44] G.N. Folefoc, J. Dwyer, J. Catal. 136 (1992) 43.
[45] L.R.R. de Araujo, M. Schmal, Appl. Catal. A 235 (2002) 139.
[46] A.C.M. van den Broek, J. van Grondelle, R.A. van Santen, J. Catal. 167 (1997) 417.
[47] H. Friedrich, P.E. de Jongh, A.J. Verkleij, K.P. de Jong, Chem. Rev. 109 (2009) 1613.
[48] R.G. Bundens, K.M. Keville, A. Huss, C.T.-W. Chu, A. Husain, US Patent 5 146 029, 1992.
[49] D.H. Olsen, E.W. Valyocsik, R.B. Calvert, Eur. Pat. Appl. 0 102 716, 1984.
[50] L. Abrams, D.R. Corbin, R.D. Shannon, US Patent 4 814 503, 1989.